The NASA High-Altitude Imaging Wind and Rain Airborne Profiler

Lihua Li, Gerald Heymsfield, James Carswell, Daniel H. Schaubert, Matthew L. McLinden, Justin Creticos, Martin Perrine, Michael Coon, Jaime I. Cervantes, Manuel Vega, Steve Guimond, Lin Tian, and Amber Emory

***Abstract*—The High-Altitude Imaging Wind and Rain Airborne Profiler (HIWRAP) is a dual-frequency (Ka- and Ku-bands), dual-beam (30° and 40° incidence angles), and conical scanning Doppler radar designed for operation on the NASA high-altitude (∼19 km) Global Hawk Unmanned Aerial System. HIWRAP was developed under the support of the NASA Instrument Incubator Program for studies of tropical storms and severe weather events. It utilizes solid-state transmitters along with a novel transmit and receive waveform scheme that results in a system with compact size, light weight, less power consumption, and lower cost compared to radars currently in use for precipitation and Doppler wind measurements. By combining volume backscattering measurements at Ku- and Ka-bands, HIWRAP is capable of imaging radar reflectivity and 3-D wind fields in clouds and precipitation. In addition, HIWRAP is also capable of measuring surface winds in an approach similar to SeaWinds on QuikSCAT. HIWRAP operating frequencies are similar to those used by the NASA Global Precipitation Measurement (GPM) Dual-frequency Precipitation Radar, making it suitable for providing airborne validation data for the GPM mission. This paper describes the scientific motivation for the development of HIWRAP as well as the system hardware, aircraft integration, and recent flight activities. Data from recent science flights are also presented.**

***Index Terms*—Clouds, dual-frequency, imaging, precipitation, radar, scanning, wind.**

I. Introduction

EXTREME weather events, such as tropical cyclones (TCs), pose significant natural threats to coastal areas and maritime interests. Three-dimensional wind measurements at high spatial and temporal resolution are critically needed for research on TCs and for improvement in intensity forecasting. In the case of TCs and other severe ocean storms, measurements of the atmospheric winds are often sparse. To date, satellite instruments cannot fully overcome this difficulty. Although the QuikSCAT (scatterometer) [1] and WindSat (radiometer) [2] instruments provide wind measurements on a global scale, they are limited to ocean surface wind measurements in precipitation-free regions. The use of spaceborne Doppler radar wind measurements would overcome these limitations considerably, but technical challenges in the implementation of Doppler wind retrieval algorithms for spaceborne radars have not been fully overcome [3], [4]. Furthermore, spaceborne measurements have the inherent limitations of low spatial resolution, short dwell time, and long revisit time that hinders their ability to provide critical information on rapidly developing TCs.

Currently, two types of sensors are used to map the 3-D wind vector within TCs: GPS dropsondes and helical-scanning Doppler radar. GPS dropsondes can be deployed rapidly, and the wind field is derived from wind vector point samples. GPS dropsondes measure more of a gust than a mean wind, and their spatial sampling is limited to a single point at each altitude. They advect with the wind, so they do not provide a true vertical profile, and the spacing between each drop is large, making it difficult to capture subscale features. Measurements of atmospheric winds using airborne Doppler radars have filled this critical data gap and have been essential to an improved understanding and forecasting of various weather events such as TCs [5]. In the past decades, a number of airborne Doppler radars were developed for the study of TCs and severe weather events [4], [6]–[8]. These radars have provided vertical and along-track [6] or cross-track [6], [7] wind measurements. Radars using helical-scanning scheme, such as the NOAA P-3 X-band tail radar [9], are capable of providing wide-volume 3-D wind measurements. However, each volume cell is only sampled at two azimuth angles both at the same incidence angle. To derive the 3-D wind speed, the fall speed of the scatters must be assumed in order to derive the two components of the horizontal wind. This reduces the accuracy of the retrieved winds.

Research over the past decade has provided rather convincing evidence that conical scanning Doppler radars on either an airborne or orbiting satellite can provide the full horizontal wind vector in precipitation and cloud regions. A study by Moore *et al.* has examined the use of a dual-beam (i.e., dual incidence angles) Ka-band conical scan spaceborne radar called Radar Wind Sounder for determining horizontal wind over the swath of the radar scan [10]. More recently, a NOAA P3-based instrument called the Imaging Wind and Rain Airborne Profiler (IWRAP) [11] with C- and Ku-band conical scan beams has

Manuscript received May 22, 2014; revised October 23, 2014 and March 22, 2015; accepted May 31, 2015. This work was supported by the National Aeronautics and Space Administration's Instrument Incubator Program.

L. Li, G. Heymsfield, M. L. McLinden, M. Perrine, M. Coon, M. Vega, and A. Emory are with NASA Goddard Space Flight Center, Greenbelt, MD 20771 USA (e-mail: lihua.li@nasa.gov).

J. Carswell is with Remote Sensing Solutions, Barnstable, MA 02630 USA.

D. H. Schaubert is with the University of Massachusetts Amherst, Amherst, MA 01003 USA.

J. Creticos is with MITRE Corporation, Bedford, MA 01730 USA (e-mail: socsuj@gmail.com).

J. I. Cervantes is with Science Systems and Applications Inc., Lanham, MD 20706 USA.

S. Guimond is with University of Maryland, College Park, MD 20742 USA (e-mail: stephen.guimond@nasa.gov).

L. Tian is with GESTAR/Morgan State University, Baltimore, MD 21251 USA.

Color versions of one or more of the figures in this paper are available online at http://ieeexplore.ieee.org.

Digital Object Identifier 10.1109/TGRS.2015.2456501

been used operationally for TC measurements. This radar scans rapidly, providing forward and aft views of the same precipitation region at different azimuth angles and incidence angles. Pixel-based analysis of these measurements has provided promising results on low-level wind fields in hurricanes. However, IWRAP was designed to fly on low-altitude aircraft (below 5 km) such as the NOAA P3, and therefore, it views only a portion of the full vertical profile of the troposphere. Nevertheless, these past studies indicate that 3-D winds can be retrieved over most of the conical-scan-covered region with an accuracy of $\sim$2.0 m/s [10].

TCs are often located in remote regions of the ocean, making manned aircraft impractical because of their limited endurance. Along with the development of new technologies, NASA's interests have more recently focused on unmanned aerial system (UAS), especially high-altitude and long endurance platforms (HALE UAS), such as the Northrop Grumman Global Hawk. Wind and precipitation measurements from high-altitude aircraft, especially long-duration UAS, are highly desirable since they provide focused measurements from remote oceanic regions with higher spatial sampling and longer observation period. The Global Hawk UAS, instrumented with remote sensors, can provide repeated passes over TCs with data sets critically needed for improved understanding and forecasting of these weather events. The recent NASA Genesis and Rapid Intensification Processes (GRIP) campaign in 2010 [12] and the Hurricane and Severe Storm Sentinel (HS3) missions in 2012 and 2013 have demonstrated the capability and effectiveness of long-duration UAS equipped with remote sensors for TC research.

Through the support of the NASA Instrument Incubator Program, NASA Goddard Space Flight Center (GSFC) has teamed with Remote Sensing Solutions (RSS) and the University of Massachusetts (UMass) Amherst, Amherst, MA, USA, to design and develop the innovative High-Altitude Imaging Wind and Rain Airborne Profiler (HIWRAP) system [13]. By combining conical scan mode measurements at two different frequency bands (Ka- and Ku-bands) and two different incidence angles (30° and 40°), HIWRAP is capable of retrieving 3-D winds from the surface to cloud top by measuring surface backscatter and volume backscatter from clouds and precipitation. HIWRAP technology advances include the development of a compact dual-frequency, dual-beam, and conical scan antenna system; development of solid-state power amplifier (SSPA) based transceivers that are capable of transmitting/receiving versatile waveforms and achieving performance comparable to conventional high-peak-power tube-based weather radar systems; and development of a high-speed digital receiver and processor to handle the complex receiving pulse sequences and high data rates resulting from multireceiver channels and conical scan.

In the following sections, we provide a brief review of the HIWRAP wind measurement concept and the measurement requirements in Section II, describe the HIWRAP system hardware in Section III, discuss HIWRAP installation, test flights, and science flights on the NASA WB-57, ER-2, and Global Hawk in Section IV, and present the calibration results in Section V.

II. Measurement Concept

HIWRAP is designed to measure tropospheric winds by collecting Doppler profiles from cloud and precipitation volume backscatter measurements. The selection of Ku- and Ka-band frequencies was based on the trade-off between hardware size, spatial resolution, backscatter efficiency, atmospheric attenuation, cost, etc. The Ku-band frequency provides reasonable storm penetration capability with less attenuation, but its backscatter efficiency and spatial resolution (with the same antenna aperture) are lower than that of the Ka-band. On the other hand, the Ka-band signal experiences more significant attenuation caused by atmospheric gas (water vapor and oxygen), ice cloud, and mixed phase particles in and above the melting layer, and by precipitation between the melting layer and the surface. However, with the use of the Ka-band, HIWRAP is more sensitive to cloud particles and small droplets than lower frequency radars, enabling it to provide 3-D winds in lower reflectivity regions of storms. In general, with conical scanning beams and slant range to the surface, the HIWRAP Ka-band signal will start to lose the surface return when the average one-way path attenuation rate is above $\sim$1.3 dB/km. This attenuation rate at Ka-band corresponds to approximately 5-mm/h rain rate and approximately 34-dBZ nominal radar reflectivity [14]. In reality, the Ka-band signal will also experience Mie scatter effects in addition to the significant path attenuation under moderate storm conditions. Therefore, the reflectivity measurements are usually lower than 34 dBZ. In this situation, less attenuated Ku-band will be used for better retrieval of radar reflectivity. HIWRAP's dual-frequency operation enables the retrieval of the particle size of clouds and precipitation by assuming a drop-size distribution. Moreover, these frequencies are similar to those used by the NASA Global Precipitation Measurement (GPM) Dual-frequency Precipitation Radar [15]. Therefore, HIWRAP is also capable of providing airborne validation data for the GPM mission. In addition to volumetric measurements from atmospheric targets, ocean surface backscatter measurements using the dual-frequency and dual conical scanning beams allow the retrieval of ocean surface vector winds similar to QuikSCAT.

As shown in Fig. 1, HIWRAP transmits and receives two Ku-band beams (30° and 40°) and two Ka-band beams (30° and 40°) simultaneously. By rotating the antenna around the vertical axis, the beams sweep through the volume beneath the aircraft and simultaneously make Doppler velocity and reflectivity profile measurements.

As illustrated in Fig. 2, for most volume cells within the swath (except those on the flight track or at cross-track positions), HIWRAP will view this cell at both Ku- and Ka-bands from two different incidence angles and four different azimuth angles (forward and backward view while the aircraft flies over the cell), from which the three components of the wind can be derived. For a detailed analysis, Guimond *et al.* has described an algorithm to retrieve the 3-D wind field using HIWRAP-type measurements [16]. In that analysis, the fall velocity of precipitation was modeled using empirical expressions based on reflectivity, and the HIWRAP Ku-band reflectivity data were used to determine the cloud or rain particle fall speeds. Due to the Global Hawk ground speed ($\sim$170 m/s) and the potentially

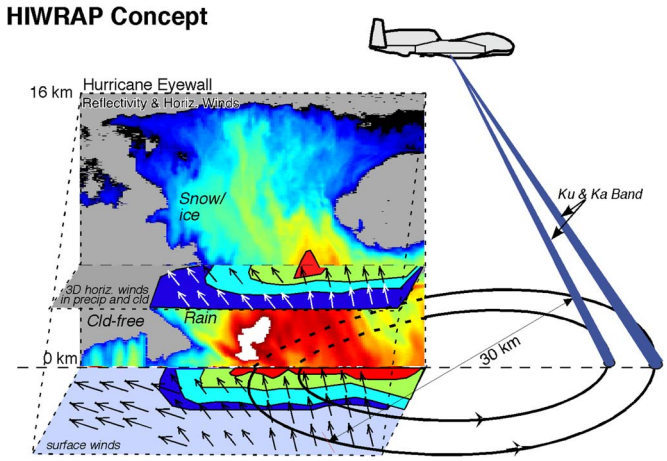

Fig. 1. By utilizing a dual-frequency dual-looking angle antenna, HIWRAP is capable of transmitting and receiving two Ku-band beams (30° and 40°) and two Ka-band beams (30° and 40°) simultaneously. By rotating the antenna around the vertical axis, the beams sweep through the volume beneath the aircraft and simultaneously make multiprofile measurements of Doppler velocity and reflectivity.

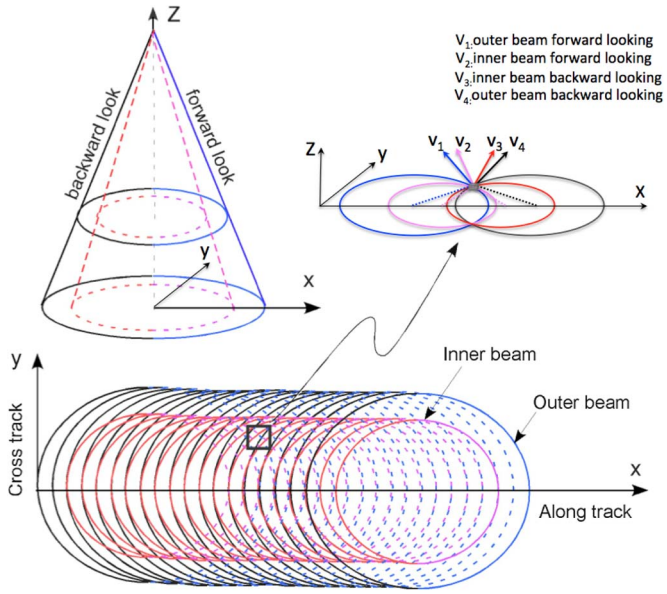

Fig. 2. While Global Hawk flies in the along-track direction, at given altitude, HIWRAP beams sweep and form two helical tracks with 30° and 40° incidence angles (at each incidence angle, there are a Ka-band beam and a Ku-band beam). For a given cell within the inner beam swath, HIWRAP will view this cell at both Ku- and Ka-bands from two different incidence angles (30° and 40°) and four different azimuth angles (forward and backward looking while the aircraft flies over the cell), from which the three components of the wind can be derived.

strong horizontal winds, the Doppler velocity measurements may be folded in some regions. Different techniques, such as dual pulse repetition frequency (Dual-PRF) and frequency diversity Doppler processing [17], could be used for unfolding Doppler velocities. When these methods do not provide a large enough velocity interval and there is still folding, an environmental wind profile is assumed for unfolding radial velocity. The measurement requirements for which HIWRAP was designed are given in Table I for wind retrievals in 1 km by 1 km by 120 m pixels. Analysis of different incidence angle combinations showed that operating at 30° and 40° incidence maximized the number of retrieval cells meeting the wind vector uncertainty requirements [17].

TABLE I
HIWRAP MEASUREMENT REQUIREMENTS

	Parameters	Range	Accuracy
Retrieval Products (resolution cell: 1km x 1km x 120m)	Horiz. Wind Speed (ms^{-1})	0-100	2.0
	Horiz. Wind Direction (°)	0-360	15
	Surface Wind Speed (ms^{-1})	0-60	2.0
	Surface Wind Direction (°)	0-360	15
	Vertical Wind Speed (ms^{-1})	± 20	2.0

TABLE II
HIWRAP SYSTEM PARAMETERS

Parameters	Specifications			
	Inner Beam		Outer Beam	
Frequency (GHz)	13.91	35.56	13.47	33.72
Tx Peak Power (W) *	25.0	8.0	25.0	8.0
Antenna Gain (dBi)	35.4	42.2	35.2	42.6
AZ 3 dB Beamwidth (°)	2.9	1.2	3.1	1.3
EL 3 dB Beamwidth (°)	3.0	1.2	2.9	1.2
Antenna Beams (°)	30.0		39.6	
Polarization	H		V	
Antenna Sidelobe (dB)	< -26.4	-27.2	< -23.2	- 26.6
PRF (Hz)	5000/4000 Dual PRF			
Pulsewidth (μs)	0-60			
Rx Bandwidth (MHz)	0-4, programmable			
Chirp Bandwidth (MHz)	0-4, programmable			
Dynamic Range (dB)	> 65			
Min. Detect. Reflectivity (dBZe, 150m range res., 10 km range, 20 μs/1 MHz chirp, 16 RPM scanning rate.)	7.8	1.5	7.8	1.5
Doppler Velocity (m/s)	0-110 (accuracy 1.5 m/s for SNR > 10)			
Scanning	Conical, 10-30 RPM			

*: The Ka-band was upgraded with a 45 W (peak power) SSPA after 2013. Upgrade on the Ku-band with an 80 W (peak power) SSPA is under way.

III. SYSTEM DESCRIPTION

The design of HIWRAP involved compromises in order to address the scientific requirements and hardware limitations imposed by the size, power, and weight constraints of the Global Hawk platform. A number of factors such as the high-altitude environment, limited space, weight, and power posed challenges to the system design. In addition, the entire radar system must have the capability to operate in autonomous mode. Table II provides the performance specifications for HIWRAP, while Fig. 3 shows the HIWRAP system block diagram. The radar hardware including the intermediate frequency and local oscillator (IF/LO) subsystem, the RF transceivers, and the digital receiver and processor are mounted on a rotating structure that typically spins at 16 r/min (Fig. 4). These subsystems on the scanner are not pressurized. The ambient temperature and pressure at nominal flight altitude (∼19 km) are about −55 °C and 1 psi under a standard atmosphere environment. To maintain the radar transceiver at optimum temperature, the transmitter power amplifiers are cooled by using heat pipes, heat sinks, and fans. The scanner motor is a dc-powered, direct-drive brushless, and commercial off-the-shelf (COTS) unit with a highly flexible programmable motor amplifier and a high-resolution encoder. It communicates with the host computer system through an Ethernet link. The rest of the radar hardware including the data system, the power

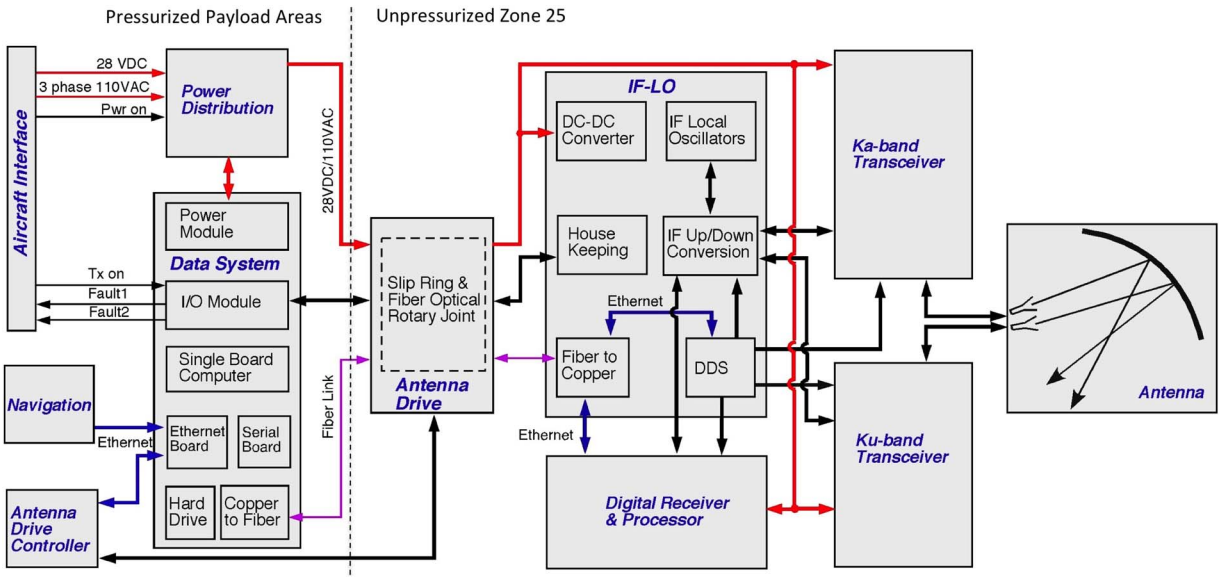

Fig. 3. HIWRAP system block diagram. The vertical dashed line is the pressure interface. The subsystems at the left side of the dashed line are located in the pressurized payload compartments on Global Hawk, while the subsystems shown at the right side of the dashed line are installed in the unpressurized radome chamber (zone 25).

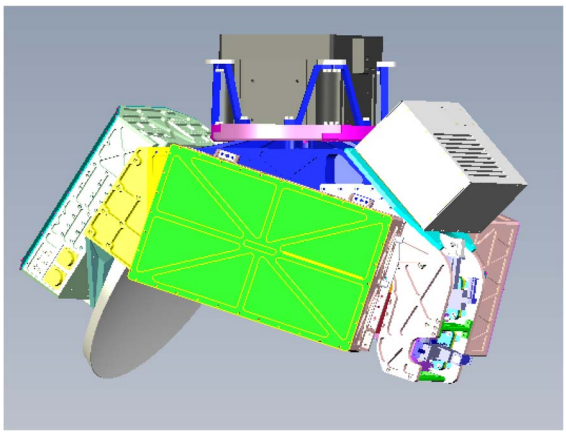

Fig. 4. HIWRAP scanner assembly, which is installed in the unpressurized radome chamber (zone 25) on Global Hawk.

distribution, the navigation unit, and the scanner controller is installed in the stationary and environmentally controlled payload areas, where the internal pressure is kept at about 4 psi while the temperature is controlled within 0–45 °C range. A commercial slip ring and a fiber optical link which includes a fiber rotary joint and media converters are used for power, I/O control, and data communication between the hardware on the scanner in the unpressurized radome bay region (zone 25) and the subsystems in the pressurized zones on the Global Hawk. This configuration avoids usage of long waveguides and a multichannel RF rotary joint, which is lossy and difficult to build and maintain at HIWRAP frequencies. The following section provides a brief description of the radar key subsystems.

A. Dual-Frequency, Dual-Looking Angle, and Conical Scanning Antenna

The HIWRAP antenna subsystem was designed by the University of Massachusetts Amherst [18], fabricated and integrated by NASA GSFC and Welch Mechanical Design. It

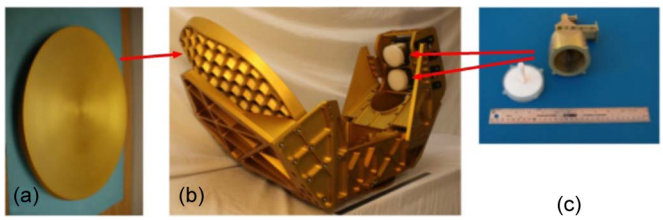

Fig. 5. HIWRAP antenna (a) main reflector. (b) Antenna assembly on the flight frame. (c) One of the dual-frequency feeds.

consists of a flight frame that also functions as the mounting structure of the radar transceiver hardware, a 20-in parabolic offset reflector, and two dual-frequency feeds to form the 30° and 40° beams. These two incidence angles (30° and 40°) were chosen based on a number of considerations that include the following: 1) enabling near optimal azimuth diversity when viewing the horizontal vector wind while measuring a significant component of vertical velocity; 2) similar incidence angle scheme for previous scatterometers enables best use of existing geophysical model functions for ocean surface wind measurements; and 3) aircraft payload constraints for implementation of two off-nadir beams. Each of the two feeds supports simultaneous operation at Ka- and Ku-bands, while the frequency of the Ka (or Ku) 30° beam is slightly different from the Ka (or Ku) 40° beam. The frequency separation between these two feeds allows HIWRAP's receivers to separate the return signals from each beam and allows simultaneous transmission on one beam while receiving from the other. The 30° incidence beams are horizontally polarized, while the 40° beams are vertically polarized. The use of orthogonal polarizations reduces wind direction ambiguity associated with ocean scatterometry [19]. The HIWRAP beam configuration is consistent with the QuikSCAT inner and outer beam polarization arrangement [2]. Table II gives the parameters for this antenna. Fig. 5 shows the precision-machined reflector, the mounting frame, and the dual-frequency feed.

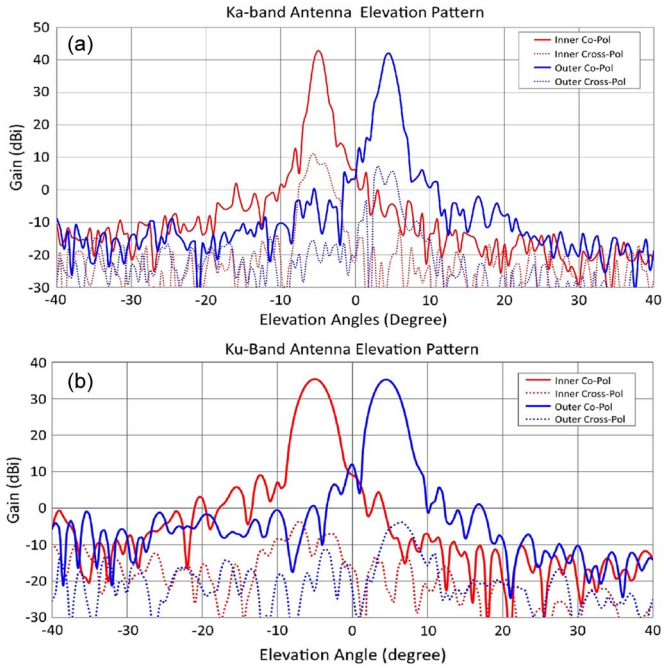

Fig. 6. HIWRAP antenna pattern. (a) Ka-band elevation. (b) Ku-band elevation. Elevation axis shifted to midway between beams. On Global Hawk, nadir direction is at the right-hand side of the patterns and 30° (inner beam) and 40° (outer beams) from the beam centers.

For an airborne downward-looking radar, surface returns coupled through the antenna sidelobes could cause contamination of the weather target signals. For the HIWRAP Global Hawk configuration, the antenna sidelobes between the main beam center to 30° (inner beams) and to 40° (outer beams) at the close to nadir direction side (right-hand side of the elevation beam patterns given by Fig. 6) need to be minimized. Fig. 6 shows that the one-way antenna sidelobes near 30° and 40° from the beam centers are approximately −55 and −47 dB below the main beams of Ka-band and Ku-band, respectively. These sidelobe values are below the required −40 dB (Ka-band) and −45 dB (Ku-band) in order to avoid surface clutter.

B. Dual-Frequency Solid-State Transceivers

The traditional tube-based radar transmitter requires a high-voltage power supply and modulator to drive a high-peak-power RF amplifier. Therefore, the radar usually requires pressurization of its transmitter and front-end subsystem for operation at high-altitude low-pressure environment. This usually results in a radar system with large size, heavy weight, and poor system reliability. Recent advancements in the communication industry have led to higher power solid-state amplifiers with average output powers comparable to that of tube-based power amplifiers. Compared to tube-based transmitters, an SSPA can be built in much more compact size with lower phase noise [20] and better amplitude stability. In addition, SSPA can be operated at much higher duty cycle (up to 100%). This enables the usage of versatile waveforms, such as frequency diversity pulses for more independent samples and long frequency-modulated chirps for pulse compression.

HIWRAP uses commercial SSPAs as its transmitters. The Ku-band subsystem utilizes a single unit power amplifier that delivers 25-W peak power, while the Ka-band subsystem uses a power combining amplifier assembly that produces 8-W peak power for each beam (Ka-band was upgraded using a single SSPA with 45-W peak power after 2013 while upgrade on the Ku-band with an 80-W peak power SSPA is under way). Direct digital synthesizer (DDS) based custom PCB board was developed to produce the transmit waveform and timing control signals. The combination of the DDS along with field-programmable gate array (FPGA) technologies enabled the software-controlled versatile waveform generation for achieving a fully programmable transmit waveform with options of frequency modulation, frequency diversity, and amplitude modulation, as well as synchronized radar timing control.

Figs. 7 and 8 show the HIWRAP Ku- and Ka-band transceiver subsystem block diagrams. The transceiver design supports simultaneous operation at two center frequencies at each band (each center frequency aligns with one of the two incidence angles) in order to maintain high temporal and spatial resolutions. Innovative approaches are taken to enhance independent sample rates and utilize the maximum duty cycle that the SSPAs can deliver. At each frequency band (Ka or Ku), both upper and lower sideband mixing products in the RF upconversion stage are used to produce the two RF channels to form the two beams. As such, this design only needs one RF local oscillator for the Ka (or Ku) subsystem, thus saving on space, power consumption, and weight. RF filters with high rejection ratio are used in the receiver to ensure the channel isolation between the inner and outer beams at each band (measured better than 70 dB). In addition, both transceivers include the noise injection loops for monitoring the receiver gain variation.

The HIWRAP transmit waveform is fully programmable, such as the scheme described by McLinden *et al.* [21]. It transmits a pulse sequence that consists of a number of pulses with slightly different center frequencies. The echo signals from these pulses are separated by the numerically controlled oscillators (NCOs) and the digital filters implemented within the FPGA-based digital receiver. The samples from these subchannels are independent; therefore, they could be integrated for achieving better system sensitivity. A similar approach has been used by other sensors, such as the National Center for Atmospheric Research ELDORA radar [10]. Fig. 9 illustrates the time domain structure of one typical waveform developed by RSS and NASA GSFC. It consists of two groups of pulses for the outer beam and inner beam, respectively. The first group (outer beam) consists of a 2-μs single tone pulse followed by a 20-μs FM chirp and then another 2-μs single tone pulse. The center frequencies of these pulses fall within the outer beam channel frequency bandwidth and are slightly offset in frequency from one another. The frequency shift allows the digital receiver to separate the simultaneous returns. When the receiver captures these signals, the first short pulse provides measurements from the surface to mid-troposphere, while the chirp pulse covers ranges from near the surface to high altitude with higher sensitivity by using pulse compression. The second single tone pulse is used to overcome the blind range near the radar caused by leakage of the chirp pulse. For regions overlapped by these pulses, data samples at the same range gate from each pulse are independent; therefore, they could be

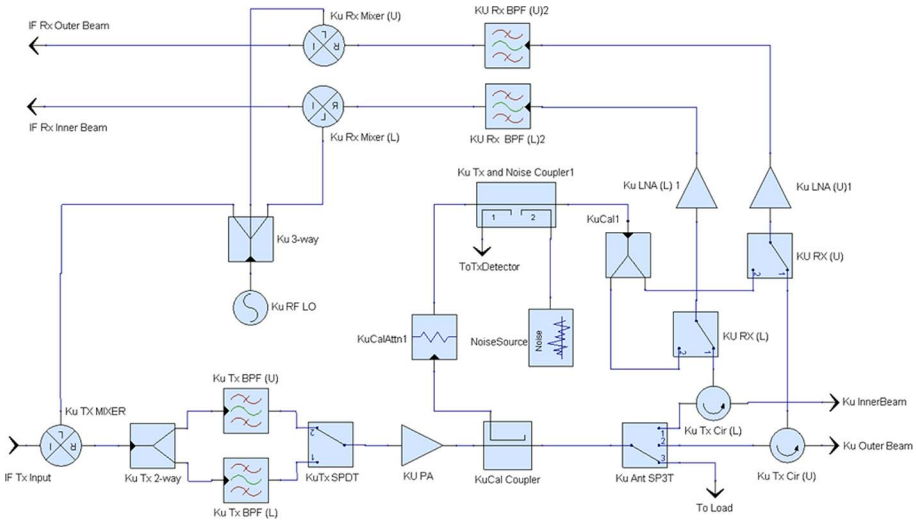

Fig. 7. HIWRAP transceiver Ku-band subsystem.

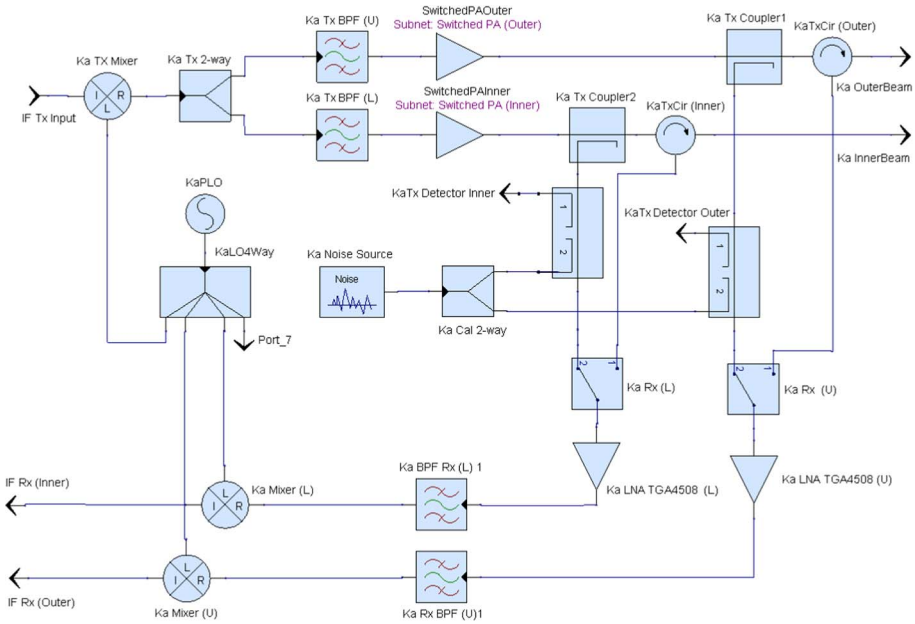

Fig. 8. HIWRAP transceiver Ka-band subsystem.

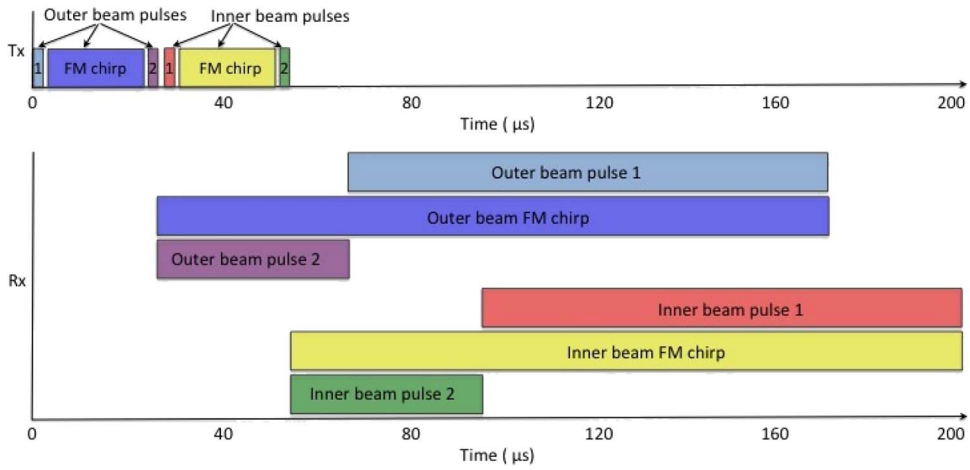

Fig. 9. Example of HIWRAP transmission and reception timing scheme.

integrated to achieve better system sensitivity. The second group of pulses (inner beam) follows the same scheme as the first group but is centered within the inner beam bandwidth. For Doppler velocity estimates, pulse-pair algorithm and dual PRF technique can be applied using different combinations of pulses to extend the unambiguous Doppler velocity up to approximately 110 ms^{-1} even though the overall PRF of the waveform sequence is only 5 kHz. Assuming a Gaussian Doppler spectrum with narrow spectrum width and large signal-to-noise ratios, the standard deviation of Doppler velocity estimate by using the pulse pair algorithm is given as $\sigma = \sqrt{\lambda \text{PRF} \sigma_v / 8M\sqrt{\pi}}$ [22], where M is the number of pulse pairs for integration, PRF is the radar transmit pulse repetition rate, and σ_v is the target spectrum width given as $\sigma_v^2 = \sigma_s^2 + \sigma_d^2 \sin^2\theta_e + \sigma_t^2 + \sigma_a^2 + \sigma_{\text{rot}}^2$, where σ_s^2 is due to shear, σ_d^2 is due to fall speed distribution, σ_t^2 is due to turbulence, σ_a^2 is due to aircraft ground speed, σ_{rot}^2 is due to antenna rotation, and θ_e is the antenna beam elevation angle [22]. Furthermore, σ_a is given as $\sigma_a = 0.3\theta v_a$, where θ is the antenna 3-dB beamwidth in radian and v_a is the aircraft ground speed in meters per second [23]. σ_{rot}^2 is given as $\sigma_{\text{rot}}^2 = \ln 2(\alpha\lambda \cos\theta_e / 2\pi\theta)^2$, where α is the antenna angular velocity in radians per second [22]. Using a similar analysis described by Heymsfield *et al.* [6], we have $\sigma_s \simeq 0.5$ m/s, $\sigma_d \simeq 1.0$ m/s, and $\sigma_t \simeq 1.0$ m/s. For HIWRAP on the Global Hawk, $v_a \simeq 170$ m/s; therefore, σ_a is about 2.7 m/s for the Ku-band beam and about 1.1 m/s for the Ka-band beam. HIWRAP antenna typically rotates at 100°/s. For 40° beams ($\theta_e = 50°$), σ_{rot} is about 0.063 m/s for the Ku-band and about 0.06 m/s for the Ka-band. The final spectrum width σ_v values for the Ku-band beam and the Ka-band beam are 3.0 and 1.7 m/s, respectively. The aforementioned analysis shows that the Doppler spectrum broaden effect due to antenna rotation is very small compared to the contribution from other factors. With $M = 128$ and PRF $= 5000$ Hz, the Ku-band standard deviation of Doppler velocity σ is calculated as 0.4 m/s, while this value for the Ka-band is approximately 0.2 m/s.

Fig. 10 shows HIWRAP system sensitivity versus range. By using combined single tone pulses and FM chirp with pulse compression, the radar achieved the system sensitivity of a conventional pulsed radar near the radar and near the surface while simultaneously enjoying increased sensitivity and range resolution by using pulse compression for the middle and high altitudes of each profile. This mitigates range sidelobe issues near the surface and the "blind zone" near the radar associated with pulse compression. Efforts are under way for further reducing the pulse compression sidelobes. In addition, SSPA technology has been further developed in the past years. SSPAs with higher output power at Ka-band and Ku-band are now available in the commercial market. The HIWRAP Ka-band transceiver has been upgraded with a 45-W SSPPA since 2013 while the Ku-band upgrade with an 80-W SSPA is under way.

C. FPGA-Based Digital Receiver and Signal Processor

The HIWRAP utilizes a high-speed digital receiver and signal processor subsystem developed by RSS. This subsystem consists of a number of custom-built modules including a high-speed backplane, a network processor card, a switch fabric card, and two digital receiver and processor cards. All of these modules are housed in a compact conduction cool cage. The digital receiver and signal processor subsystem is responsible for implementing digital in-phase and quadrature-phase (I&Q) detection, match filtering (i.e., pulse compression), spectral and/or pulse-pair processing, and data reduction through data profile averaging. It uses Xilinx Virtex-5 FPGAs along with a multigigabit network processor to provide the most compact solution possible without a requirement for pressurization. This subsystem is network based so that the data can be easily ingested by a PC-based data system where further processing algorithms may be applied.

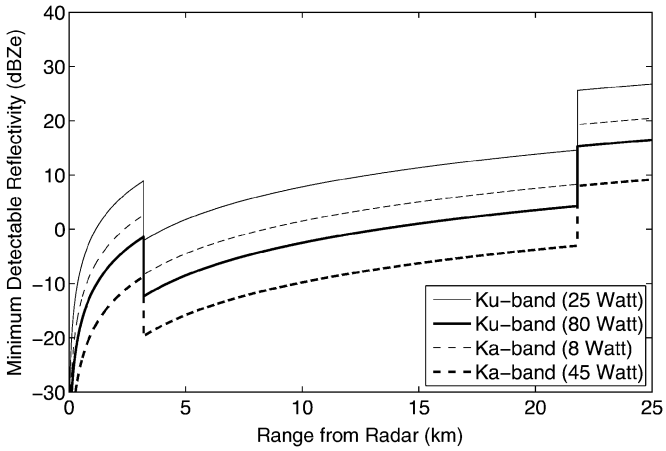

Fig. 10. HIWRAP minimum detectable reflectivity (not attenuation corrected) versus range with 150-m range resolution. The original SSPAs used by HIWRAP have peak power levels of 8 and 25 W at Ka-band and Ku-band, respectively. The Ka-band was upgraded with a new SSPA with 45-W peak power after 2013. The Ku-band upgrade with an 80-W SSPA is under way.

Another novel feature of this FPGA-based digital receiver is that each IF channel will support up to eight independent subchannels, with more than 90 dB of rejection for frequencies beyond 1.5 times of the bandwidth from the center frequency of the given subchannel. By using a programmable digital waveform generator and an FPGA-based digital receiver for data acquisition and data processing, HIWRAP is able to transmit a pulse sequence that consists of a number of pulses with slightly different center frequencies. The echo signals from these pulses are separated by the NCOs and digital filters implemented within the digital receiver. The primary digital receiver characteristics are the following:

1) two IF channels per board and up to eight independent subchannels per IF channel;
2) 500-kHz to 20-MHz bandwidth per subchannel, 40-MHz aggregated bandwidth per IF channel;
3) 14-b A/D resolution;
4) multigigabit data transfer rate;
5) matched filter supports up to 30-dB pulse compression gain per subchannel;
6) supports up to 1000 range gates.

D. 3U Compact PCI-Based Data System and Fiber Optic Ethernet Link

The HIWRAP data system utilizes two commercially available Compact PCI (CPCI) backplanes along with a single board

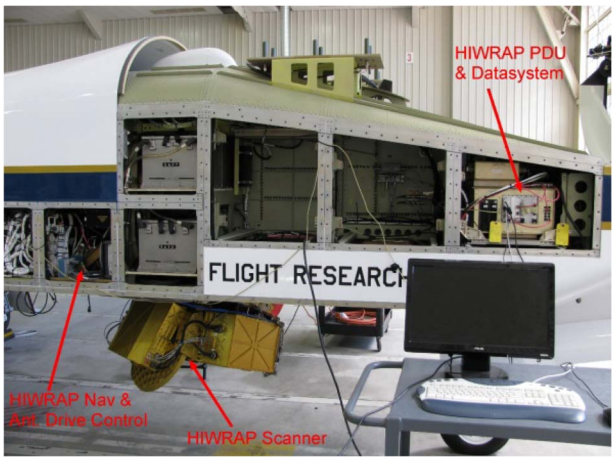

Fig. 11. HIWRAP installation on NASA Global Hawk.

computer (SBC) on each backplane. One SBC runs the radar control program and captures housekeeping and radar data from the digital receiver through a high-speed fiber optic/gigabit Ethernet link, and the other one processes a subset of radar data in real time and sends the processed data products to ground through the Global Hawk satellite downlink. A multifunction I/O card is utilized for radar control and housekeeping data communication. A commercial fiber optic Ethernet link provides communication between the radar hardware on the scanner and the hardware on the stationary (pressurized) side of the payload. HIWRAP also utilizes a dedicated high-speed navigation system that provides precise platform position/altitude information on the local network. Radar status information, scanner position, navigation data, and radar data are collected and saved on a solid-state disk array by the host computer.

IV. Field Deployment and Flight Missions

HIWRAP was originally designed to fly on the NASA Global Hawk, but it is also compatible with other NASA high-altitude aircraft, such as the WB57 and ER-2 (nadir mode only). Because of limited Global Hawk availability when the instrument was completed, HIWRAP was first installed on the NASA WB-57 aircraft based at NASA Johnson Space Center in March 2010 for initial tests of the instrument performance and the measurement concept. The test flights on the WB57 proved that HIWRAP mechanical hardware, thermal control, and radar electronics performed well in the high-altitude environment and provided valuable information for preparing the radar for Global Hawk flights.

After the WB57 test flights, HIWRAP was integrated on the NASA Global Hawk AV-6 in support of the NASA GRIP science flight mission in the summer of 2010 [14]. Fig. 11 shows the HIWRAP scanner along with radar subsystems installed in the Global Hawk payload zone 25, while the power distribution unit and the data system were installed in payload zone 12. A radome fairing and a dual-frequency radome were designed and fabricated for HIWRAP operation.

During the GRIP mission, the Global Hawk carried out five science flights. These flights include Hurricane Frank on the Pacific coast, Hurricane Earl on the Atlantic U.S. east coast, Hurricane

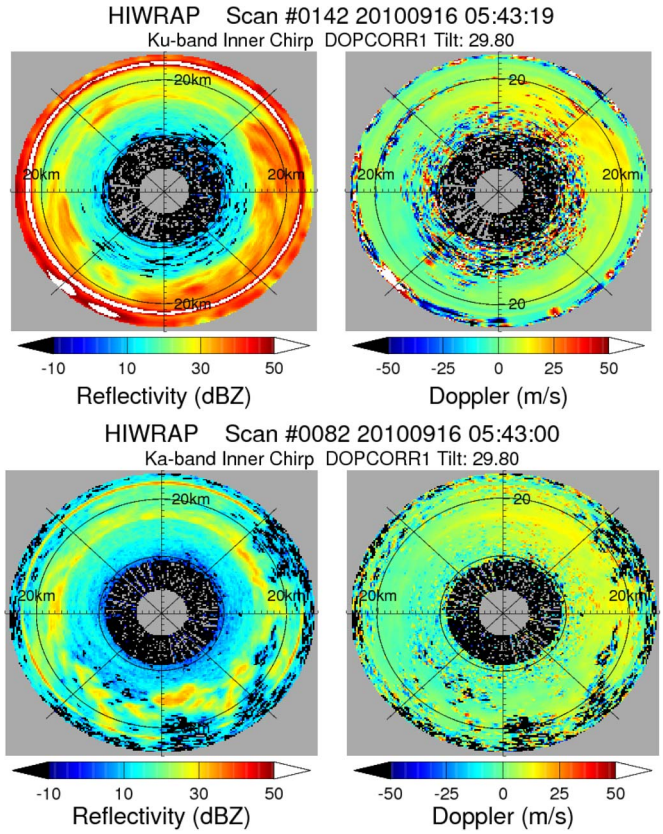

Fig. 12. Azimuthal plots (a) radar reflectivity and (b) Doppler velocity corrected for aircraft motions for Ku inner beam (top) and Ka inner beam (bottom). These data were measured by the 20 μs/1 MHz FM chirp subchannels.

Karl before tropical storm development in the Caribbean and then as a hurricane in the Gulf of Mexico, and Hurricane Matthew in the Caribbean prior to landfall in Central America. More details on these flights during GRIP were described by Braun *et al.* [14]. The Global Hawk enables long flight range to reach remote ocean areas and long staging time over the storm system, therefore significantly improving the amount of science data that an onboard instrument can collect. Compared to operation on manned aircraft, such as the NASA WB57 and ER-2, the longer duration flights on the Global Hawk also pose new challenges in terms of instrument control, thermal management, and data communication. HIWRAP performed well during these 15- to 25-h GRIP science flights with progressively better performance each flight. During the Karl flights, the Global Hawk demonstrated its capability of flying over the top of hurricanes and made 20 overpasses of the hurricane eye (in comparison, the manned NASA ER-2 typically makes a few overpasses during each flight). Fig. 12 shows the polar format images of radar reflectivity and Doppler velocity measured by the Ka inner beam and Ku inner beam channels (20 μs/1 MHz FM chirp) over one scan cycle as the Global Hawk passed over this storm. The center of each plot is the radar location at approximately 19 km altitude; the Global Hawk flight direction is toward the top of the page. The images show a precipitation region up to about 10 km slant range and a melting layer at about 5 km slant range, as well as surface return at about 20–23 km slant range. The variation in the range of the surface return was due to approximately 2° aircraft pitch angle. The Ka-band image

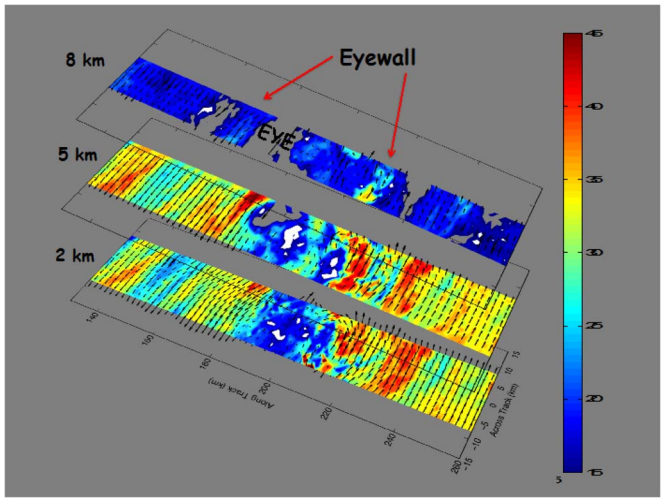

Fig. 13. Horizontal wind fields in Hurricane Karl (2010) at three different altitudes using the algorithm described in Guimond *et al.* [16]. The colors denote the Ku-band reflectivity, and the black arrows show the horizontal wind vector.

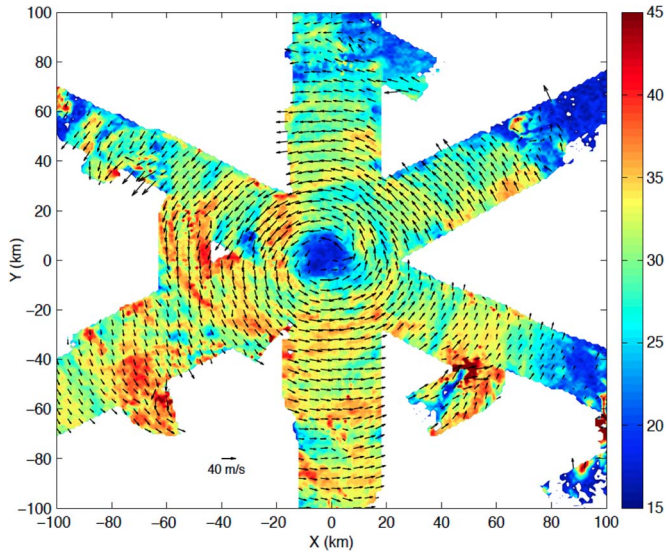

Fig. 14. Horizontal wind fields in Hurricane Karl during GRIP at 3-km altitude using a combination of 17 flight tracks.

also indicates strong attenuation from precipitation for example at 45° azimuth. As a result, the surface is not seen in Ka-band returns in these highly attenuating regions. Doppler velocities have been estimated using the pulse-pair method, and they have been unfolded using a dual PRF technique. The Doppler velocities shown in Fig. 12 represent the speed of liquid and ice particles in the storm with the aircraft motion contribution removed from the data. No antenna sidelobe has been observed in these images.

A wind field retrieval algorithm was developed and described by Guimond *et al.* [16] using Doppler velocities measured by HIWRAP from different beams and different view angles. In that analysis, retrievals of the three Cartesian wind components over the entire radar sampling volume are described, which can be determined using either a traditional least squares or variational solution procedure. The random errors in the retrievals due to the airborne radar geometry and noise in the Doppler velocities are evaluated using both an error propagation analysis with least squares theory and a numerical simulation of a hurricane. The fall velocity of precipitation was modeled using empirical expressions and the HIWRAP Ku-band reflectivity measurements. Fig. 13 illustrates an example of the horizontal wind field at three different altitudes during one flight line across Hurricane Karl on September 17, 2010, during GRIP. These analyses show that the vertical and along-track wind errors have strong across-track dependence with values ranging from 0.25 m/s at nadir to 1.0 and 2.0 m/s at the swath edges, respectively. The average across-track wind errors are ∼2.5 m/s or 7% of the hurricane wind speed.

Fig. 14 shows storm-centered composite wind fields at 3 km height from 17 flight tracks across Hurricane Karl. Some of these flight tracks are short in duration. At the end of each track, the Global Hawk made turns, and the data during the turns were not included due to the large variation of aircraft pitch and roll angles. These wind fields reveal important inner-core structures of the hurricane, including details on deep convective processes and rain bands.

In the Spring of 2011, HIWRAP was installed on the NASA ER-2 with a fixed nadir-pointing dual-frequency lens antenna to support the NASA GPM Ground Validation (GV) Midlatitude Continental Convective Clouds Experiment (MC3E) mission. The ER-2 carried out ten science and calibration flights during the MC3E mission. Figs. 15 and 16 show radar reflectivity images measured by HIWRAP Ku- and Ka-band channels from May 24, 2011, respectively. In both figures, the top panel is the image from the pulse compression subchannel, while the bottom panel is the image of the single tone short pulse subchannel. The range sidelobe in the pulse compression subchannel is due to the limited time-bandwidth product used during this field campaign. Even though HIWRAP is capable of supporting large time-bandwidth pulse compression for better range sidelobe reduction, the choice of chirp pulsewidth and bandwidth for each operation is a trade-off between blind range, system sensitivity, data rate, and range sidelobe performance. For the HIWRAP initial science missions (GRIP and MC3E), the digital receiver algorithm was still under development, and pulse compression implementation was focused on increasing sensitivity. The chirp and receiver bandwidth was set to 1 MHz in order to keep the system data rate within the limit for multichannel operation. With a 20 μs/1 MHz chirp, the pulse compression gain through MC3E flights was approximately 13 dB. There was up to 3-dB SNR loss due to amplitude tapering. The final pulse compression gain is ∼10 dB, and the range sidelobe was about −32 dB compared to the main lobe. For operation that requires even lower range sidelobe, larger time-bandwidth product and different amplitude modulation on the chirp can be used. Efforts to further reduce the range sidelobe effect are under way.

In Figs. 15 and 16, the short pulse channel was used to zoom in the near surface target to overcome the range sidelobes in the pulse compression channel using the approach described by McLinden *et al.* [21]. The images show attenuation due to the intense convective core from 21:38 to 21:40 UTC in the Ku-band images and from 21:38 to 21:42 UTC in the Ka-band

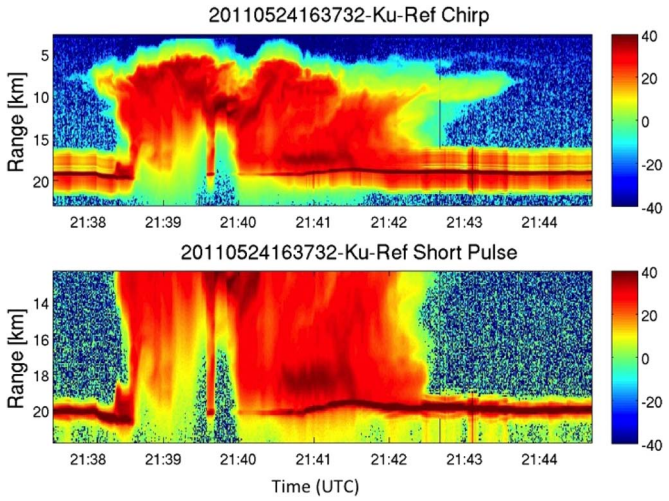

Fig. 15. HIWRAP Ku-band reflectivity measured by the pulse compression channel (top) and the single tone short pulse channel (bottom) from a severe hailstorm on May 24, 2011. The strong radar return near 20 km radar range is the surface return. The images show a very strong attenuation of the radar signal from 21:38 to 21:40 UTC so that the surface is not seen. More detailed data analysis on HIWRAP MC3E data is described by Heymsfield *et al.* [24].

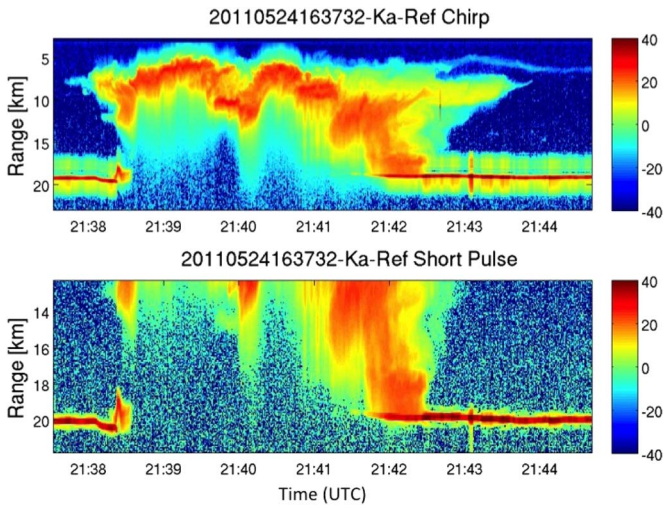

Fig. 16. HIWRAP Ka-band reflectivity from the pulse compression channel (top) and the single tone short pulse channel (bottom) on May 24, 2011. This reflectivity image also indicates a strong attenuation at Ka-band 21:38 to 21:42 UTC.

images, so that the surface was not seen. The Ka-band chirp channel image (top panel of Fig. 16) also shows a thin outflow layer of cirrus from 21:42 to 21:44 UTC at ∼15-km altitude. This indicates good sensitivity at this frequency.

V. Radar Calibration

HIWRAP calibration is implemented in three steps: 1) system calibration using the parameters of individual components; 2) using the ocean surface return as an external reference similar to that reported by Li *et al.* [25] and Tanelli *et al.* [26]; and 3) internal calibration using a pulse-by-pulse correction during postflight data processing as described by Sadowy [27]. These approaches are independent to each other and provide a self-consistent check to ensure the accuracy of the final calibration

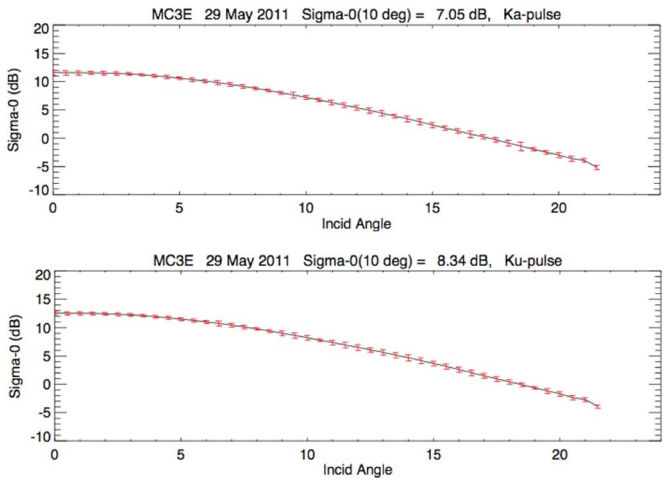

Fig. 17. Ocean surface σ_0 versus incidence angle from one calibration flight on May 29, 2011.

result. Step 1) is a straight calculation using the radar range equation described by Doviak and Zrnic [22] along with component specifications, and steps 2) and 3) are based on radar measurements.

During MC3E, two calibration flights were carried out over the Gulf of Mexico near the Texas/Louisiana coast. Although HIWRAP was configured as fixed nadir pointing, the ER-2 flew 0° to 20° roll angle banks and circle pattern with a constant roll angle near 10°. Ocean backscatter from 0 to 20° incidence angles was measured by HIWRAP beams. Radar surface returns from the chirp pulse are used to estimate the normalized radar cross section (NRCS) since the surface foot print was beam filled for this channel and therefore eliminates the uncertainty in using a short pulse for surface NRCS measurements [28]. Atmospheric attenuation at HIWRAP frequencies was calculated and corrected using meteorological data from adjacent buoys. Fig. 17 shows σ_0 versus incidence angle for Ku- and Ka-bands. The results near 10° incidence angle agree with that reported by Tanelli *et al.* [26] and the ocean surface NRCS models within 1.0 dB.

Although the internal calibration does not include the front-end Tx/Rx circulator and antenna, it couples an attenuated transmit pulse into the receiver and provides pulse-by-pulse measurements of the full transfer function of the transceiver. The components not included in the calibration loop are passive, and their performance is stable and usually straightforward to measure and also can be verified using the ocean surface return. Once radar system calibration is carried out and verified through all of the aforementioned approaches, radar science data are then calibrated using the internal calibration pulse collected during each transmit cycle.

VI. Summary

HIWRAP is a solid-state transmitter-based, dual-frequency (Ka- and Ku-bands), dual-beam (30° and 40° incidence angles), and conical scan Doppler radar system. It was designed for operation on the NASA high-altitude (∼19 km) Global Hawk for measurements of tropospheric and ocean surface winds as well as to study cloud and precipitation microphysical properties

such as particle size and water content. Flights that have already occurred on the Global Hawk during GRIP and the Hurricane Severe Storm Sentinel (HS3) campaigns have shown the potential of HIWRAP for providing repeated passes over TCs to produce information on the structure of the storms. Data measured by HIWRAP through GRIP have shown promising results for wind field retrievals. HIWRAP is also compatible with the other NASA high-altitude aircraft including the ER-2 and WB57. To this end, HIWRAP has successfully been flown on all of the aforementioned three different types of NASA high-altitude aircraft. Recent flights on the ER-2 for GPM ground validation have provided valuable information on convective storms. Future plans are to fly additional flights on the Global Hawk for HS3 and on the ER-2 for GPM postlaunch ground validation campaign. On data analysis, efforts will be focused on 3-D in storm wind fields as well as ocean surface wind retrievals.

As the first SSPA-based airborne weather radar, HIWRAP has successfully demonstrated its unique capability for remote sensing research. In comparison, traditional weather radar is usually built with a tube-based transmitter, which requires a high-voltage power supply and modulator. This usually results in a radar system with large size, heavy weight, and poor system reliability. SSPA is much more compact in size. It offers better RF phase and amplitude performance and high reliability. Although the achievable RF peak power with the current SSPA technology is still one or two magnitudes lower than the tube-based power amplifier at the same frequency, the high duty cycle capability of SSPA enables the use of long FM chirp for pulse compression, which makes the overall system sensitivity of SSPA-based radar comparable to the traditional high-peak-power tube-based radar. In addition, SSPA supports programmable versatile transmission waveforms, which provide options of multimode operation, better range resolution, frequency diversity pulses for extended Doppler Nyquist range, and more independent data samples. SSPA technologies have achieved remarkable improvement in the past decade. The SSPAs used by HIWRAP are built with GsAs devices. The new GaN technology has enabled the development of SSPAs with even higher RF power and higher efficiency. The most significant challenge of using SSPA for atmospheric radar is pulse compression range sidelobe reduction, especially for airborne and spaceborne applications. The strong surface return could couple through the range sidelobe and contaminate the weather signals near the surface. The most recent digital waveform generation technology and advanced pulse compression techniques, such as adaptive pulse compression, have shown promising results to achieve an ultralow range sidelobe. It is believed that the advances in digital waveform generation, digital receivers, and SSPAs have opened a new era for the development of compact and high-performance airborne and spaceborne remote sensing radars.

ACKNOWLEDGMENT

The authors would like to thank the funding support from the NASA Instrument Incubator Program during HIWRAP development, and supports from the NASA Global Hawk, ER-2, and WB-57 groups during HIWRAP test flights and field missions.

REFERENCES

[1] C. Wu *et al.*, "The SeaWinds scatterometer instrument," in *Proc. IEEE IGARSS*, Pasadena, CA, USA, Aug. 8–12, 1994, pp. 1511–1515.
[2] P. W. Gaiser *et al.*, "The WindSat spaceborne polarimetric microwave radiometer: Sensor description and early orbit performance," *IEEE Trans. Geosci. Remote Sens.*, vol. 42, no. 11, pp. 2347–2361, Nov. 2004.
[3] F. D. Marks and R. A. Houze, "Inner core structure of Hurricane Alicia from airborne Doppler radar observations," *J. Atmos. Sci.*, vol. 44, no. 9, pp. 1296–1317, May 1987
[4] G. M. Heymsfield *et al.*, "The EDOP radar system on the high altitude NASA ER-2 aircraft," *J. Atmos. Ocean. Technol.*, vol. 13, no. 4, pp. 795–809, Aug. 1996.
[5] F. D. Marks and L. K. Shay, "PDT-5, USWRP PDT-5 Report, 1998: Tropical Cyclones: Forecast problems and associated research opportunities," *Bull. Amer. Meteorol. Soc.*, vol. 79, no. 2, pp. 305–323, 1998.
[6] S. L. Durden *et al.*, "ARMAR: An airborne rain-mapping radar," *J. Atmos. Ocean. Technol.*, vol. 11, no. 3, pp. 727–737, Jun. 1994.
[7] G. A. Sadowy, A. C. Berkun, W. Chun, E. Im, and S. L. Durden, "Development of an advanced airborne precipitation radar," *Microw. J.*, vol. 46, no. 1, pp. 84–98, Jan. 2003.
[8] P. H. Hildebrand, C. A. Walther, C. Frush, J. Testud, and G. Baudin, "The ELDORA/ASTRAIA airborne Doppler weather radar," *Proc. IEEE*, vol. 82, no. 12, pp. 1873–1890, Dec. 1994.
[9] D. P. Jorgensen and J. D. DuGranrut, "A dual-beam technique for deriving wind fields from airborne Doppler radar," in *Proc. 25th Int. Conf. Radar Meteorol., Amer. Meteorol. Soc.*, Paris, France, 1991, pp. 458–461.
[10] R. K. Moore, B. Beh, and S. Song, "Scanning for a satellite radar wind sounder (RAWS)," in *Proc. IGARRS Remote Sens. Sustain. Future*, 1996, pp. 996–998.
[11] D. Fernandez *et al.*, "IWRAP: The imaging wind and rain airborne profiler for remote sensing of the ocean and the atmospheric boundary layer within tropical cyclones," *IEEE Trans. Geosci. Remote Sens.*, vol. 43, no. 8, pp. 1775–1787, Aug. 2005.
[12] S. A. Braun *et al.*, "NASA's Genesis and Rapid Intensification Processes (GRIP) field experiment," *Bull. Amer. Meteorol. Soc.*, vol. 94, no. 3, pp. 345–363, Mar. 2013.
[13] G. M. Heymsfield, J. Carswell, L. Li, D. Schaubert, and J. Creticos, "Development of the High-Altitude Imaging Wind and Rain Airborne Profiler (HIWRAP)," in *Proc. NSTC*, College Park, MD, USA, Jun. 19–21, 2007. [Online]. Available: http://esto.nasa.gov/conferences/nstc2007/papers/Carswell_James_B5P2_NSTC-07-0085.pdf
[14] S. Matrosov, "Attenuation-based estimates of rainfall rates aloft with vertically pointing Ka-band radars," *J. Atmos. Ocean. Technol.*, vol. 22, pp. 43–54, 2005.
[15] M. Kojima *et al.*, "Dual-frequency Precipitation Radar (DPR) development on the Global Precipitation Measurement (GPM) core observatory," in *Proc. SPIE*, 2012, vol. 8528, Art. ID. 85281A.
[16] S. R. Guimond, L. Tian, G. M. Heymsfield and S. J. Frasier, "Wind retrieval algorithms for the IWRAP and HIWRAP airborne Doppler radars with applications to hurricanes," *J. Atmos. Ocean. Technol.*, vol. 31, no. 6, pp. 1189–1215, Jun. 2014.
[17] J. R. Carswell, "Final report: A revolutionary wind and rain airborne profiler for unmanned aircraft vehicles," NASA Small Bus. Technol. Transfer, Washington, DC, USA Final Rep., Contract No. NNG05CA96.
[18] J. P. Creticos, "Development and design of dual-band, multi-function remote sensing antennas," Ph.D. dissertation, Dept. Elect. Comput. Eng., Univ. Massachusetts Amherst, Amherst, MA, USA, 2008.
[19] S. H. Yueh andW. J. Wilson, "Polarimetric radar remote sensing of ocean surface wind," *IEEE Trans. Geosci. Remote Sens.*, vol. 40, no. 4, pp. 793–800, Apr. 2002.
[20] S. M. Haque, D. J. Hoppe, L. W. Epp, "Solid state power amplifier and travelling wave tube amplifier additive phase noise characterization at Ka-band operation," in *Proc. IEEE Radar Conf.*, Pasadena, CA, USA, 2009, pp. 1–4.
[21] M. McLinden *et al.*, "Utilizing versatile transmission waveforms to mitigate pulse compression range sidelobes with the HIWRAP radar," *IEEE Trans. Geosci. Remote Sens. Lett.*, vol. 10, no. 6, Nov. 2013, pp. 1365–1368.
[22] R. J. Doviak and D. S. Zrnic, *Doppler Radar and Weather Observations*. New York, NY, USA: Academic, 1993.
[23] D. Atlas, "Advances in radar meteorology," in *Advances in Geophysics*, vol. 10. New York, NY, USA: Academic , pp. 317–478, 1964.
[24] G. M. Heymsfield, L. Tian, L. Li, M. McLinden, and J. I. Cervantes, "Airborne radar observations of severe hailstorms: Implications for future spaceborne radar," *J. Appl. Meteorol. Climatol.*, vol. 52, pp. 1851–1867, 2013.
[25] L. Li, G. M. Heymsfield, L. Tian, and P. E. Racette, "Measurements of ocean surface backscattering using an airborne 94-GHz cloud radar—Implication for calibration of airborne and spaceborne W-band radars," *J. Atmos. Ocean. Technol.*, vol. 22, no. 7, pp. 1033–1045, Jul. 2005.
[26] S. Taneli, S. L. Durden, E. Im, "Simultaneous measurements of Ku- and Ka-band sea surface cross sections by an airborne radar," *IEEE Geosci. Remote Sens. Lett.*, vol. 3, no. 3, pp. 359–363, Jul. 2006.

[27] G. A. Sadowy, "A 95 GHz airborne cloud radar: Statistics of cloud reflectivity and analysis of beam-filling Errors for a proposed spaceborne cloud radar," Ph.D. dissertation, Dept. Elect. Comput. Eng., Univ. Massachusetts Amherst, Amherst, MA, USA, 1999.
[28] I. J. Caylor, G. M. Heymsfield, R. Meneghini, and L. S. Miller, "Correction of sampling errors in ocean surface cross-sectional estimates from nadir-looking weather radar," *J. Atmos. Ocean. Technol.*, vol. 14, no. 1, pp. 203–210, Feb. 1997.

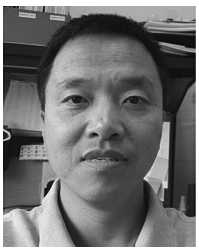

Lihua Li received the B.S. degree from Tsinghua University, Beijing, China, in 1988, the M.S. degree from the Chinese Academy of Sciences, Beijing, in 1991, and the Ph.D. degree in electrical and computer engineering from the University of Massachusetts (UMass) Amherst, Amherst, MA, USA, in 2000.

He has been with the Microwave Instrument Technology Branch (MITB), NASA Goddard Space Flight Center (GSFC), Greenbelt, MD, USA, since 2008. At GSFC, he has led the development of a number of remote sensing radars for research application on the NASA high-altitude aircraft, including WB57, ER-2, and Global Hawk. He has served as the PI and Co-PI of a number of research projects as well as the Instrument Scientist of the spaceborne Global Precipitation Measurement Dual-frequency Precipitation Radar. Before joining GSFC, he was with the Goddard Earth Science and Technology (GEST) Center, University of Maryland, Baltimore County (UMBC), Baltimore, MD, from 2001 to 2008. He was the Principal Engineer of the HIWRAP, EXRAD, CRS, and ER-2 Doppler Radar (EDOP) systems. Prior to joining GEST, he was a Research Engineer (2000–2001) with the Microwave Remote Sensing Laboratory (MIRSL), UMass Amherst. He served as the Engineer Lead for the ground-based cloud profiling radar system and the JPL/UMass Airborne Cloud Radar. He is the author or coauthor of approximately 20 journal publications.

Dr. Li is a member of the American Meteorological Society.

Gerald Heymsfield received the M.S. degree in geophysical sciences from the University of Chicago, Chicago, IL, USA, in 1972 and the Ph.D. degree in meteorology from the University of Oklahoma, Norman, OK, USA, in 2006.

He was then a Research Associate with the University of Chicago from 2006 to 2009. In 1979, he joined the Goddard Space Flight Center Laboratory for Atmospheric Sciences, and he has worked there as a Research Meteorologist for 36 years. He has led the high-altitude airborne radar efforts at Goddard that now include three radars. His research interests include radar and satellite meteorology with emphasis on severe storms including hurricanes.

Dr. Heymsfield was the recipient of the NASA Exceptional Scientific Achievement Medal in 2008.

James Carswell received the B.S.E.E. degree from Tufts University, Medford, MA, USA, in 1990 and the Ph.D. degree in electrical engineering from the University of Massachusetts (UMass) Amherst, Amherst, MA, in 1995.

He is the Cofounder and President of Remote Sensing Solutions, Inc., and an Adjunct Professor with the UMass. As the Cofounder and President of Remote Sensing Solutions, he serves as a principal investigator and technical leader in providing radar systems and digital processing and data management solutions for remote sensing applications. He leads the development of an FPGA-based digital receiver (iRAP) for the NASA High-Altitude Imaging Wind and Rain Airborne Profiler (HIWRAP) that is deployed on the NASA Global Hawk UAV and ER-2 aircraft. He designed the solid-state Ku/Ka-band transceiver for HIWRAP. He has developed several solid-state airborne and ground-based Doppler radars for atmospheric and oceanic research. As the Lead System Engineer, he designed and developed high-altitude multichannel Ka-band interferometric radars for centimetric-level topography mapping. He is currently leading efforts to develop and deploy interferometric digital beamforming millimeter-wave airborne radars and ultrawideband millimeter-wave profiling radars for situational awareness, mapping, and security applications. He has worked in the area of microwave and millimeter-wave remote sensing since 1991.

Daniel H. Schaubert received the Ph.D. degree in electrical engineering from the University of Illinois, Champaign, IL, USA.

He is a Professor Emeritus of electrical engineering and the former Director of the Center for Advanced Sensor and Communication Antennas, University of Massachusetts, Amherst, MA, USA. He worked at the U.S. Army Research Laboratory and the U.S. Food and Drug Administration prior to joining the University of Massachusetts in 1982. His contributions have been mainly in the areas of antenna design and analysis. He has patents for conformal and printed circuit antennas. Several of his antenna designs have been used in military and civilian systems for radars, radiometers, and communications, and he has designed low-cost antennas for commercial cellular and local area network products. He directed the design, fabrication, and testing of antennas for the cloud profiling radar system, a polarimetric 33- and 95-GHz mobile radar, and the High-Altitude Imaging Wind and Rain Airborne Profiler, a dual-beam 13- and 35-GHz airborne radar. He led the design efforts for several multioctave scanning array antennas, including the first prototypes for the Thousand Element Array demonstrator of the Square Kilometer Array project.

Dr. Schaubert was the President of the IEEE Antennas and Propagation Society, an Associate Editor of the IEEE TRANSACTIONS ON ANTENNAS AND PROPAGATION, the Secretary–Treasurer of the Society, a *Newsletter* Editor, and the Membership Chairman. He organized the annual Antenna Applications Symposium. He received the Distinguished Alumni Award from the Department of Electrical and Computer Engineering, University of Illinois, the IEEE John Kraus Antenna Award, the H. A. Wheeler Prize Applications Paper Award, and the IEEE Third Millennium Medal. He was an advisor to the European Antenna Centre of Excellence and was a member of the executive team for the IET Antenna and Propagation Professional Network.

Matthew L. McLinden received the B.Sc. and M.Sc. degrees in electrical and computer engineering from the University of Massachusetts Amherst, Amherst, MA, USA, in 2006 and 2010, respectively.

He is a Research Engineer with the Microwave Instrument Technology Branch and High-Altitude Radar Group, NASA/Goddard Space Flight Center, Greenbelt, MD, USA. At NASA, he has supported the Aquarius and GPM satellite missions as well as three airborne radars, namely, HIWRAP, CRS, and EXRAD. He is the Lead Engineer of the NASA Cloud Radar System. His primary research interests are active and passive microwave remote sensing of atmospheric phenomena from airborne and spaceborne platforms.

Mr. McLinden is a member of the American Meteorology Society. He received the NASA Early Career Achievement Medal in 2015.

Justin Creticos received the B.S.E.E. degree from Union College, Schenectady, NY, USA, and the M.S.E.C.E. and Ph.D. degrees from the University of Massachusetts Amherst, Amherst, MA, USA.

He is a Group Leader at MITRE Corporation. Prior to working at MITRE, he was a Research Assistant with the Center for Advanced Sensor and Communication Antennas, University of Massachusetts Amherst.

Martin Perrine received the B.S.E.E. degree from Michigan State University, East Lansing, MI, USA, in 1984 and the M.S.E.E. degree from Johns Hopkins University, Baltimore, MD, USA, in 1987.

He is a Senior Electrical Engineer with NASA Goddard Space Flight Center, Greenbelt, MD, supporting radar and communication system and architecture development. Prior to joining NASA, he worked on the regulation of radio systems for the Federal Communication Commission and developed radio systems for the Department of Defense.

Michael Coon received the B.S. degree in computer engineering from the University of Maryland, Baltimore County, Baltimore, MD, USA, in 2010 and the M.S. degree in electrical and computer engineering from Johns Hopkins University, Baltimore, in 2013.

He is a Radar Engineer with the Microwave Instrument Technology Branch, NASA/Goddard Space Flight Center (GSFC). At GSFC, he has been involved in the development and upgrade of multiple airborne remote sensing instruments, including the High-Altitude Imaging Wind and Rain Airborne Profiler, ER-2 X-band radar, and cloud radar system.

Jaime I. Cervantes received the B.S. degree in aerospace engineering from the University of Texas at Austin, Austin, TX, USA. He is currently working toward the M.S. degree in computer science at Johns Hopkins University, Baltimore, MD, USA.

He is a Staff Research Scientist with Science System and Applications, Inc. (SSAI), providing onsite support at Goddard Space Flight Center. He is currently involved in the development of the High-Altitude Imaging Wind and Rain Airborne Profiler and the ER-2 X-band radar. He also provides engineering support for the Tropospheric Wind Lidar Technology Experiment. His experience includes software system engineering, digital signal processing, computer graphics, and parallel computing.

Manuel Vega received the B.S.E.E. and M.S.E.E. degrees from the University of Puerto Rico, Mayagüez, Puerto Rico.

He is a Radar Engineer with the Microwave Instrument and Technology Branch, NASA Goddard Space Flight Center (GSFC), Greenbelt, MD, USA. Since joining GSFC, he has been involved in the development of Ka-band, Ku-band, X-band, and L-band airborne and ground-based radar systems.

Steve Guimond received the Ph.D. degree in atmospheric science from Florida State University, Tallahassee, FL, USA, in 2010.

He is an Assistant Research Scientist with the University of Maryland Earth System Science Interdisciplinary Center, working at Goddard Space Flight Center as a Contractor. His research includes remote sensing of clouds and precipitation with a focus on airborne Doppler radar including techniques for retrieving geophysical variables, hurricane dynamics with a focus on the role of small scales, and numerical modeling of problems with various layers of complexity from dynamic core to full physics.

Lin Tian received the Ph.D. degree in atmospheric science from the University of Chicago, Chicago, IL, USA, in 1997.

Her research interests are in the remote sensing of cloud and precipitation using radars and developing algorithms for 3-D wind retrieval from airborne Doppler radar observations.

Amber Emory received the M.S. degree in atmospheric science from Texas A&M University, College Station, TX, USA, in 2007 and Ph.D. degree in wind science and engineering from Texas Tech University, Lubbock, TX, USA, in 2012.

She is a Research Meteorologist with the NASA Goddard Space Flight Center, Greenbelt, MD, USA. She is a Principal Investigator for the X-BADGER radar system, which is a vertically pointing dual-polarimetric ground-based 3-cm wavelength radar. Her research interests include using ground-based radars and airborne radiometers to study clouds and precipitation in severe storms and tropical cyclones, the environments and kinematics of transitioning mesoscale convective systems in West Africa and the Eastern Atlantic, and hurricane initiation and rapid intensification.